Probing skin pigmentation changes with transient absorption imaging of eumelanin and pheomelanin

Dan Fu
Princeton University
Department of Chemistry
Princeton, New Jersey 08544

Tong Ye
Thomas E. Matthews
Duke University
Department of Chemistry
Durham, North Carolina 27708

James Grichnik
Duke University
Department of Medicine
Durham, North Carolina 27710

Lian Hong
John D. Simon
Duke University
Department of Chemistry
Durham, North Carolina 27708

Warren S. Warren
Duke University
Department of Chemistry and Radiology
Durham, North Carolina 27708

Abstract. As some of the most ubiquitous and biologically important natural pigments, melanins play essential roles in the photoprotection of skin. Changes in melanin production could potentially be useful for clinical diagnosis of the progression stage of melanoma. Previously we demonstrated a new method for imaging melanin distribution in tissue with two-color transient absorption microscopy. Here we extend this study to longer wavelengths and show that we are able to image melanin in fixed thin skin slices with higher signal-to-noise ratios (SNRs) and demonstrate epimode imaging. We show that both photothermal effects and long-lived excited states can contribute to the long-lived signal. Eumelanin and pheomelanin exhibit markedly different long-lived excited state absorption. This difference should enable us to map out their respective distribution in tissue samples with subcellular resolution. This technique could provide valuable information in diagnosing the malignant transformation of melanocytes. © *2008 Society of Photo-Optical Instrumentation Engineers.* [DOI: 10.1117/1.2976424]

1 Introduction

Early detection of melanoma is a long-standing challenge in clinical dermatology. The current diagnosis method based on histopathology results is lengthy and painful, and varies largely depending on the expertise of the pathologist. Over the last decade, noninvasive optical *in vivo* spectroscopy through linear absorption, Raman, and fluorescence has shown potential in the diagnosis and characterization of human skin diseases.[1–3] These methods can provide a variety of biophysical properties of cutaneous molecular markers such as melanin, hemoglobin, collagen, and lipids, but they can only explore the surface, and give far worse spatial resolution than histopathology (except confocal-based methods, which are discussed later). Therefore, it is desirable to develop a noninvasive high-resolution deep tissue imaging method with improved sensitivity and diagnostic accuracy for melanocytic skin cancer.

Currently the most developed and promising approach is reflectance mode confocal laser scanning microscopy (rCLSM). CLSM images the skin by exploiting microscopic biological variations in refractive indexes. Components of skin whose refractive indexes are higher than the average refractive index of epidermis, such as keratin in the stratum corneum, hydrated collagen, and melanin, provide molecular and structural contrast in backscattered light. In particular, melanin granules have a high refractive index (1.7) compared with the surrounding cytoplasm (1.35), providing a strong endogenous contrast for rCLSM imaging of melanocytes.[4] The imaging depth with rCLSM is typically limited to less than 350 μm.[5] The morphological features indicated by melanocyte distribution as well as cell shape and cell size provide important diagnostic differentiation between benign and malignant melanocytic skin lesions.[6–8] However, rCLSM also suffers from a few drawbacks. For example, the scattering measurement is not background free and is not specific to melanin. Langerhans cells may appear as melanocytes in the epidermis.[9]

Another important feature that is often missing from optical-imaging-based diagnostic methods is the molecular aspects of melanogenesis (the production of melanin in specialized organelles called melanosomes) in the malignant transformation of skin lesions. Two types of melanins are generally found in skin:[10,11] eumelanin, a black or dark brown insoluble material, and pheomelanin, a yellow or reddish-brown alkali-soluble material. Both types are synthesized within melanosomes belonging to melanocytes, and distributed through dendritic extensions of the melanocytes to surrounding epidermal

Address all correspondence to Warren S. Warren, Duke Univ., Dept. of Chemistry and Radiology, Durham, NC 27708; E-mail: warren.warren@duke.edu

cells (keratinocytes), resulting in pigmentation of the skin. One of the major functions of melanin pigmentation is generally believed to be shielding the skin from harmful ultraviolet radiation (UVR). However, there is considerable evidence suggesting that pheomelanin or its precursors play an important role in carcinogenesis/mutagenesis.[12] This may arise because pheomelanin is more vulnerable than eumelanin to UVR, thus generating free radicals and leading to DNA damage and increased mutagenicity.[13,14] This implies that people with different pigments would be expected to have varying risk factors for developing skin cancer or melanoma, as supported by epidemiological studies.[15] In addition, it has also been shown that the production of pheomelanin is increased significantly in melanoma and melanocytic nevi compared with normal skin.[16,17] Therefore, the differentiation of eumelanin and pheomelanin in skin tissue can provide information about changes in melanogenesis and potentially be useful for clinical diagnosis of the progression stage of melanoma.[18]

Previously we have demonstrated a pump-probe-type imaging method to specifically map the melanin distribution in cells with high sensitivity.[19] This method has all the advantages of other multiphoton imaging techniques, such as inherent sectioning capabilities and high sensitivity. Moreover, it is much more specific to endogenous melanocytic features than rCLSM. Here we improve on our previous study with longer pump-probe wavelengths. More importantly, we studied the long-lived signal in detail and showed that both photothermal effects and long-lived excited states could contribute to this signal. Eumelanin and pheomelanin exhibited markedly different long-lived signals both in their lifetimes and in the ratio of short-lived to long-lived signal. We also demonstrated epi-mode imaging using human hair as the model system. Utilizing these differences in microscopic study, we should be able to determine the eumelanin and pheomelanin distribution in skin tissues with high resolution. This work could open a new window in the study of melanogenesis and transformation of melanocytes from normal to malignant.

2 Materials and Methods

2.1 Sample Preparation

Skin samples. Deidentified fixed human skin slides (unstained) were obtained from the Department of Dermatology at Duke University Medical Center. All the skin slides have corresponding histopathology results. Skin slice thickness is about 5 μm.

Hair samples. Indonesian, black human hair was purchased from R. Parrino Hair Goods (Northport, New York). Red human hair samples were obtained from a 20 year-old female locally (Durham, North Carolina), and the hair had never been permed or dyed. Chemical degradation analysis of melanosomes from those hair samples showed a dominant eumelanin content with undetectable pheomelanin in the black hair melanosomes, while the red hair melanosomes contained a mixed type melanin, predominantly pheomelanin, with a low eumelanin content.[10,11]

Phantom sample. A simple phantom containing a capillary tube (inner diameter=100 μm, outer diameter=170 μm) containing 30-mM R6G solution, a red hair with a diameter of

130 μm, and a dark hair with a diameter of 84 μm was made. The three specimens were immersed in immersion oil (Cargille Laboratory, Cedar Grove, NJ) and placed in close proximity to allow imaging of all three in a single frame.

Melanosome samples. Melanosome samples were isolated from black and red human hairs according to the literature.[20] For melanosome imaging experiments, melanosomes were suspended in a drop of immersion oil and sandwiched between a precleaned microscope slide and coverslip. The application of immersion oil was necessary to prevent photodamage of the samples.

2.2 Two-Color Transient Absorption Measurements

We used a simple modified pump-probe method to study the transient absorption imaging of melanin samples. The experimental setup has been described previously.[19,21] Utilizing a high frequency modulation transfer technique, we are able to sensitively detect 10^{-6} transient absorption changes in a transient absorption measurement, which is much better than typically measured with an amplified laser system, with the additional advantage of much lower power levels. This is extremely important for biological imaging applications due to both peak power and average power damage concerns.[22] Here we made some modifications to the original setup. The apparatus of our two-color transient absorption measurement is shown in Fig. 1. It resembles the traditional pump-probe experimental setup. A small fraction of the output of a mode-locked Ti: sapphire laser (Tsunami, 80 MHz, 100 fs, from Spectra Physics, Mountain View, CA) was intensity modulated sinusoidally with an acousto-optical modulator (AOM, from Crystal Technology, Palo Alto, CA) at 2 MHz. It was used as the pump pulse with a center wavelength of 810 nm and sent through a mechanical delay stage. The pulse train from a synchronously pumped optical parametric oscillator (Spectra Physics, Opal, 80 MHz, 120 fs, output wavelength tunable from 1300 to 1600 nm) was frequency doubled by a 1.5-mm-thick β-barium borate crystal (BBO) outside the cavity. The second harmonic at 740 nm was used as the probe. The pump and probe beams were then combined on a dichroic mirror (DCXR760, from Chroma, Rockingham, VT) and sent into a home-built laser scanning microscope (scanning mirror from Cambridge Technology, Olympus PlanApo 20$\times$ objective with NA=0.70). Before entering the objective, the two beams passed through a polarizing beamsplitter to allow only *p* polarization to pass. The sample was placed on an aluminum plate attached to a motorized *xyz* stage (Newport, Irvine CA). The detection setup was composed of a three-element lens system to refocus the probe beam, a bandpass filter (HQ710/130, Chroma) to remove the pump beam, and a large area amplified photodiode (PDA55 from Thorlabs, Newton, NJ) to detect the signal. For epidetection, backscattered light reflected by the polarizing beamsplitter was also refocused, filtered, and detected with an avalanche photodiode (APD, from Hamamatsu Bridgewater, NJ). The photodiode outputs were then sent to a rf lock-in amplifier. Since lock-in detection is phase-sensitive, both the amplitude and the phase of the modulation signal (represented by *x* and *y* channel signals at the output of the lock-in amplifier) can be obtained. We sent both *x* and *y* channel signals to a DAQ acquisition card
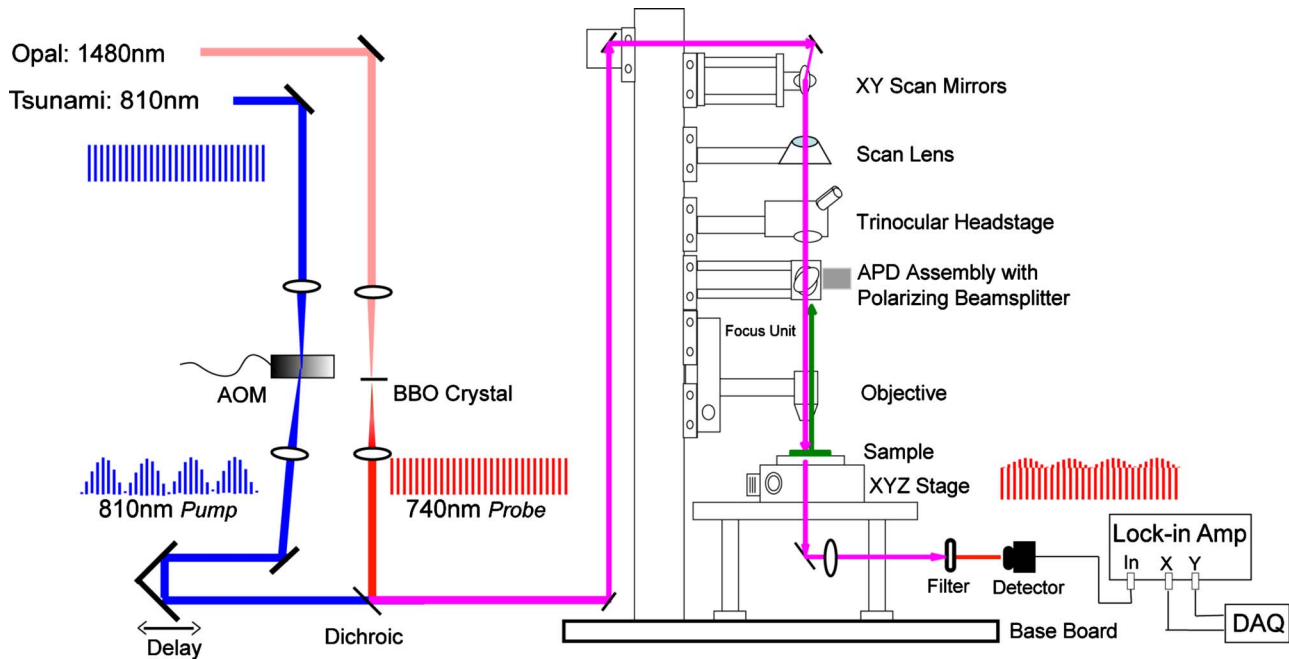
Fig. 1 Schematic view of our two-color transient absorption laser scanning microscope. AOM: acousto-optic modulator. APD: avalanche photo-diode. DAQ: data acquisition card.

(6115E DAQ board, from National Instruments, Austin, TX). All data acquisition and data analysis were done with home-built software written in Labwindows/CVI 7.1 (National Instruments) and Matlab 6.5 (Mathworks, Natick, Massachusetts).

3 Results and Discussion

3.1 In Vitro Imaging of Melanin in Skin Samples

Previously we have demonstrated imaging of melanin in B16 melanoma cells. Here with longer pump and probe wavelengths, we demonstrated imaging of fixed thin skin slices in transmission mode at a higher signal-to-noise ratio (SNR) with even less optical power than our previous study. Figure 2(a) shows the mosaic image of five bright field images of an invasive melanoma skin tissue sample (some artifacts are present at the sides of the images due to nonuniform illumination). The epidermis and dermis are on the lower side of the black line (edge of stratum corneum, which is marked with blue ink). Although not stained, the melanin granules still can be observed along the basal layer as yellow to brown particles in the image. Unlike normal skin, melanomas include an increased density of pleomorphic melanocytic cells. Figure 2(b) shows the corresponding mosaic image of five laser scanning images (only the *x* channel signal is shown) based on our two-color transient absorption microcopy technique. The SNR of the image is around 50 at 2.8-mW pump power and 1.1-mW probe power. It reveals far more detail of the melanin granules' distribution than the bright field image. We can clearly delineate the stratum corneum (seen as a bright line due to strong signal from the blue ink mark) and the basal cell layer separating the epidermis from the dermis, which is easily identified as a thick layer of bright melanin dots with the typical papillary ridges of the dermis. In the center and left

side of the image, tumor cells are also present in the dermis. Figures 2(c) and 2(d) show higher resolution images obtained with a 40× objective (Olympus UPlanFLN 40×, NA=0.75) at two different locations [marked with orange boxes in Fig. 2(b)]. The left image shows numerous cells that are irregular in size and shape, forming a large mesh in a melanin pigmentation network. The separation between epidermal and dermal compartments is very unclear. The right image shows much more uniformly oval-shaped cells primarily restricted to the
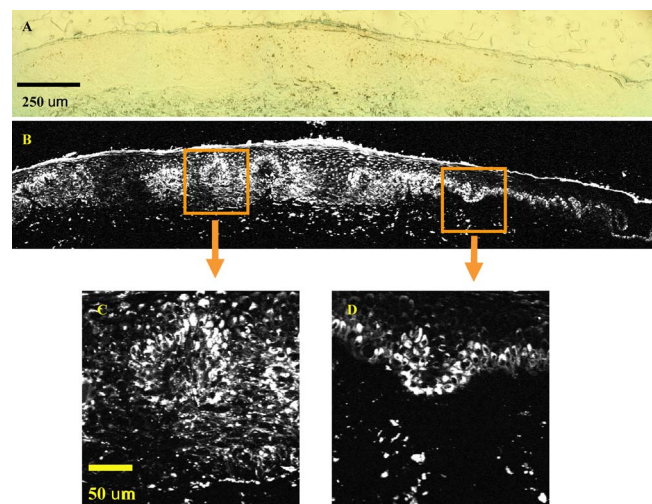
Fig. 2 Mosiac of five images of an invasive melanoma skin slice in the (a) bright field taken with a DCM 130 camera, and (b) laser scanning mode acquired with two-color transient absorption microscopy. (c) and (d) show higher magnification two-color transient absorption images taken with a 40× objective at the two locations indicated with the orange boxes. (Color online only.)

Red hair   Black hair

100 um

R6G

(a)   (b)
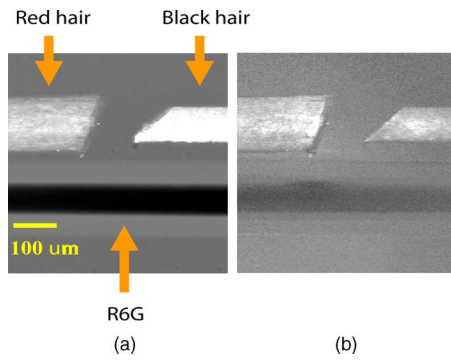
Fig. 3 (a) Transmission mode and (b) epimode transient absorption imaging of black hair with 810-nm pump and 740-nm probe at zero interpulse delay.

epidermis; potentially melanoma cells at an earlier tumor stage. These nonuniform melanin features might be useful in the diagnosis of melanoma *in vivo* and may represent different growth stages.

3.2 Epimode Imaging of Melanin

Transmission mode imaging is not a viable solution in many cases. In principle, for thick tissue imaging, any probe photons backscattered after the focus carry exactly the same modulation information as transmitted photons, which are also scattered multiple times before reaching the detector. Therefore, epimode imaging for a thick sample is entirely possible and should provide identical information to transmission mode imaging. However, unlike fluorescence, the backscattered light is at the same wavelength as the excitation light. Therefore the dichroic mirror has to be replaced with a polarizing beamsplitter to separate the backscattered light. We set the polarization of the pump and probe beam to *p* polarization so they can pass the polarizing beamsplitter completely. When the light enters tissue, some of the photons will be backscattered and depolarized. The *s* polarization component of the backscattered light can then be reflected by the polarizing beamsplitter and detected with an APD.

We imaged hair samples to demonstrate the viability of epimode imaging. Figure 3 shows transmission and epimode images of a phantom sample containing a R6G capillary tube, black hair, and red hair at zero interpulse delay. Image size is

512×512 μm. We can see that epimode images can also be used for high resolution imaging, although with a deteriorated SNR of 9 compared to that of 110 in transmission mode. This is partly due to not enough scattering in the sample. With thicker samples, we expect to have larger SNR. The difference in contrast is because the amount of light that is scattered (or transmitted) and effectively detected is not uniform across the whole field of view. The R6G solution has the least amount of scattering (or reflection from glass), while the red hair with a larger diameter is the most scattering. With bulk tissue samples, this problem should be minimized within a small imaging area. From the phase of the signal at zero delay, we can infer that at these wavelengths, the signals from both red hair and black hair are due to bleaching because they are opposite in phase compared to the R6G's known two-photon absorption signal. This is different from the previous study at shorter pump-probe wavelengths.[19]

3.3 Photothermal Effects and Long-Lived Excited States

In the previous study, we have seen that there is a signal preceding zero interpulse delay in the *x* channel as well as a constant signal in the *y* channel, independent of interpulse delay.[19] This is commonly seen in all melanin samples. Since our laser repetition rate is 80 MHz, a negative delay is essentially the same as a very long delay of about 12 ns. Therefore, we conclude that there is a long-lived component that gives rise to the amplitude and the phase of signals at negative delays. Several different mechanisms could contribute to this long-lived signal: 1. the excited state initially formed by the pump pulse went into another long-lived excited state through intersystem crossing; 2. the pump pulse heats up the sample and induces an absorption change of the probe pulse; 3. the pump pulse heats up the sample and forms a thermal lens, therefore changing the focusing of the probe pulse. The third mechanism does not change the total probe intensity but only changes its focusing. The signal arises from imperfect collection of the probe beam (equivalent to an aperture). For a thin sample, the phase of this signal should depend on whether the beam focus is before or after the sample, which can be easily measured with a *z* scan.[23] Figure 4 shows the *z* scan results of a thin layer of black hair melanosomes on a microscope slide at zero delay. The optical power deposited on the sample is 1.4 mW for the pump and 0.5 mW for the probe. Owing to
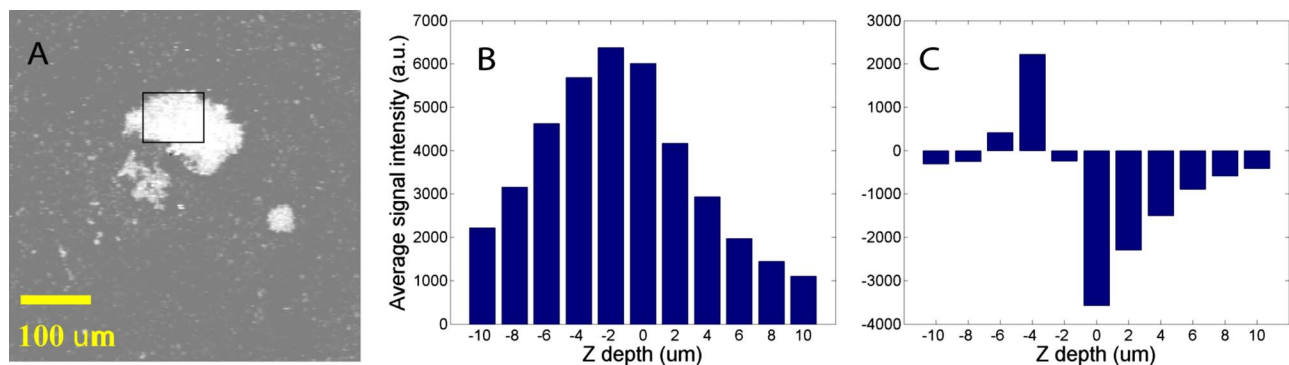
Fig. 4 (a) Transient absorption image of black hair melanosome sample. (b) and (c) show the average signals in the ROI [marked with black box in (a)] with respect to *z* depth in the *x* and *y* channels, respectively.
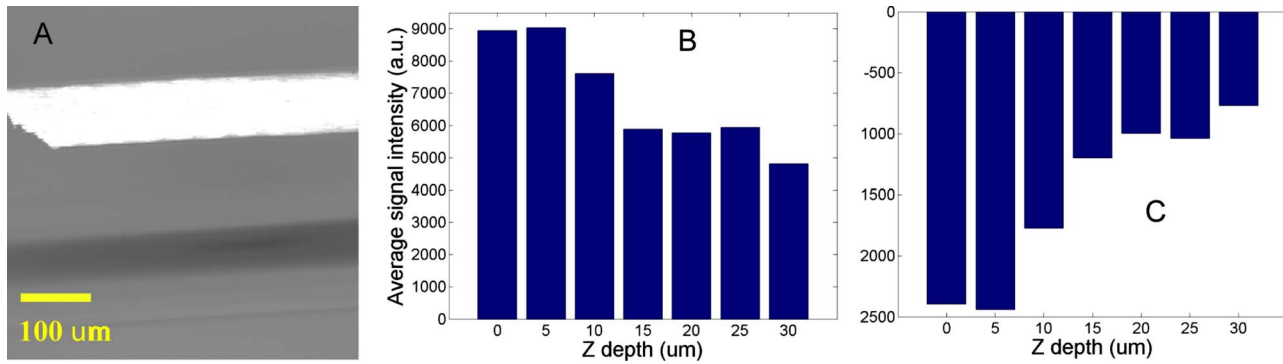
Fig. 5 (a) Transient absorption image of black hair sample. (b) and (c) show the average signals in the ROI [marked with black box in (a)] with respect to z depth in the x and y channels respectively.

the change of sign in the y channel signal in the z scan, the thermal lensing effect must be present. However, this does not exclude other possible contributions. For a thick sample, the thermal lensing effect should disappear, because multiple scattering will disrupt the phase information of the transmitted probe and therefore eliminate most of the residual thermal lensing effect. Figure 5 shows the z scan results of a black hair sample at zero delay. We can see that the phase of the y channel signal does not change sign over the scan range, which suggests that the thermal lensing effect is mostly eliminated.

To further determine whether the origin of the long-lived signal is related to the second mechanism (heating effect), we did a ratio analysis by offsetting the pump-probe beam overlap. Unlike electronic excitation of the molecules, a heating effect is not localized at the focus because of heat diffusion, which typically occurs on a time scale of 0.25 to 1 μs.[24] If we assume the long-lived signal is caused by heating effects, because it is a steady-state effect, the amount of signal is not determined by the instantaneous heating but by the thermal gradient formed. If the pump-probe beam foci have a slight offset, the ratio of the signal at long delay time (~ 12 ns) to the excitation-localized shorted-lived signal will increase. Figure 6 shows the signals of the red hair sample at various delays for both maximum overlap and slight offset of the pump probe beams (by changing the direction of probe beam

slightly at the dichroic mirror). The ratio of long-lived signal (-2 ps) to short-lived signal (0 ps) calculated for red hair at maximum overlap is 0.107, while the corresponding ratio for offsetted overlap is 0.105. The closeness of these two ratios suggests that the long-lived signal is not primarily from heating effects, but from real excited states, similar to the short-lived signal.

3.4 Differentiating Eumelanin and Pheomelanin in Tissue

It has been a long-standing challenge in pigment cell research to quantify the distribution of melanins in skin tissue *in vivo* because of their complex nature. Extracted melanins have been extensively studied using a wide variety of techniques, such as high performance liquid chromatography (HPLC),[25] electron microscopy,[26] and spectrophotometric methods.[27,28] However, these methods require very complicated and lengthy preprocessing of the sample. They are also invasive and cannot provide *in situ* microscopic information. Two-photon fluorescence and two-photon absorption microscopy of melanins has previously been studied and utilized in microscopic imaging.[29,30] However, no attempt was made to differentiate eumelanin from pheomelanin. With our highly sensitive two-color transient absorption measurement, we are now able to distinguish them with different phase behaviors.
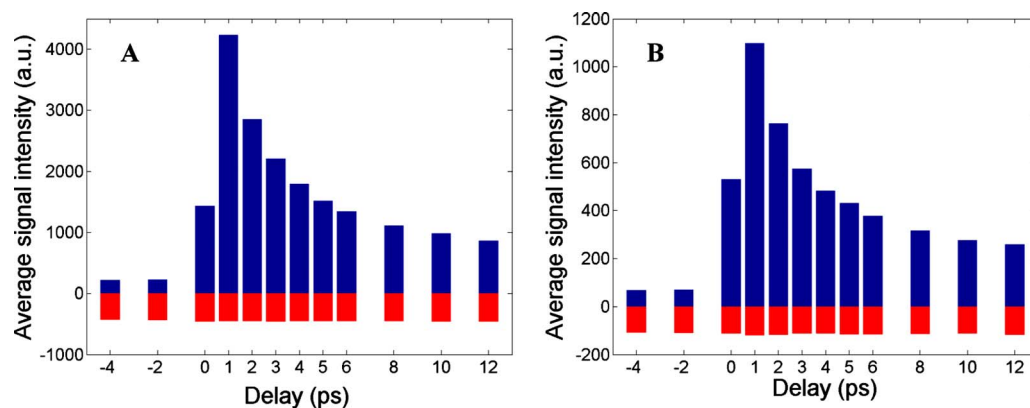
Fig. 6 Average signals of red hair with respect to interpulse delays when (a) the pump-probe beam foci have maximum overlap, and (b) the pump-probe beam foci have spatial offset.
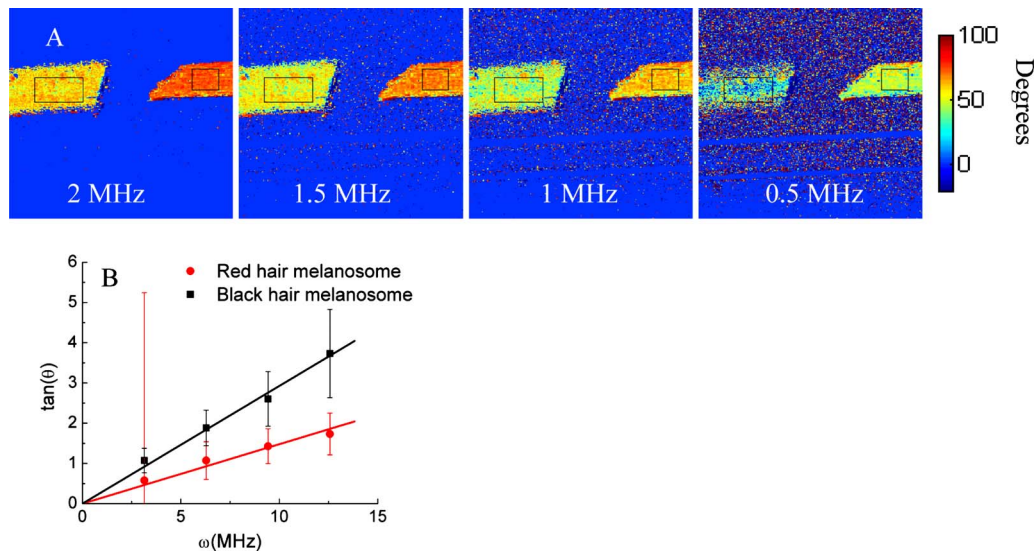
Fig. 7 (a) Phase images of the hair samples at different modulation frequency. (b) Linear fitting of the long-lived excited state lifetimes for red and black hair melanosomes.

It is interesting to compare the long-lived excited state lifetimes for different hair samples. With the same phantom sample used in the previous section, scanning images of black hair and red hair samples were acquired at various modulation frequencies. We can use the simple model $\tan(\theta)=\omega\tau$ to calculate the lifetime based on the change of phase in the signal, similar to frequency domain fluorescence lifetime measurements.[31] For each image at a different modulation frequency, we can calculate the phase θ from the x and y channel signals. The absolute phase images are plotted in Fig. 7, and we can clearly see that black hair and red hair have different phase images (for R6G, the phase is always zero because there is no long-lived signal). To calculate the lifetimes of the long-lived excited states, we used linear regression fitting of average $\tan(\theta)$ in selected regions of interests (ROIs, marked with black boxes) against the modulation frequency $\omega=2\pi f$. The resulting lifetime for red hair is 0.148 (±0.007) μs, while for black hair it is 0.293 (±0.007) μs. It should be mentioned that the lifetimes measured could also be dependent on the surrounding oxygen concentration (in this experiment, the samples were exposed to ambient air before im-

mersed in the oil for imaging). This result also confirms our conclusions that the effect is not predominantly thermal, as a thermal contribution might have different magnitudes for the two different samples, but would surely have the same decay constant.

Another important difference for red and black hair samples is in the ratio of long-lived signal to short-lived signal, which is directly proportional to the efficiency of intersystem crossing. Figure 8 shows the averaged x and y channel signals for both red hair and black hair samples with respect to interpulse delay. The long-lived signal size can be calculated with both the x and y channel signal before zero delay, while the short-lived signal can be approximated as the maximum x channel signal. The calculated ratio for red hair is around 0.1, while for black hair it is around 0.5.

As we can see, the long-lived excited state lifetime and ratio of long-lived to short-lived signal can be easily distinguished between the two types of melanosome. This opens up the possibility of doing differential imaging of eumelanin and pheomelanin in tissue.
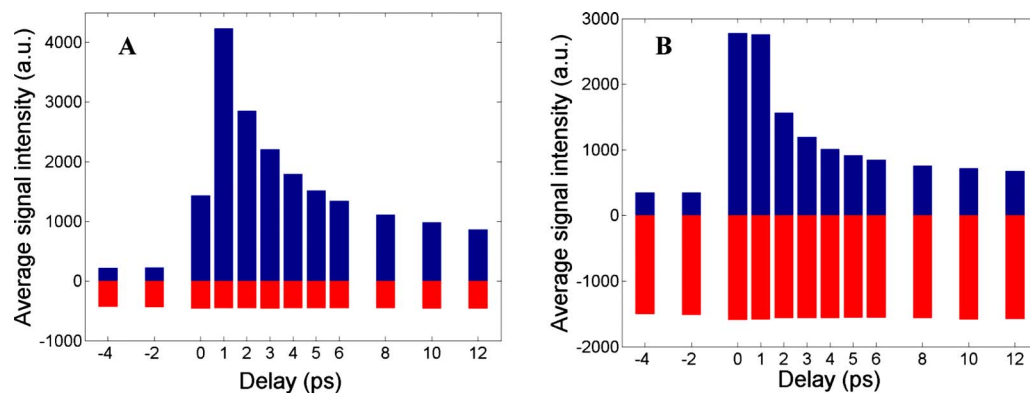
Fig. 8 Comparison of the ratio of long-lived signal to short-lived signal for (a) pheomelanin (red hair) and (b) eumelanin (black hair).

4   Conclusions

This work demonstrates the feasibility of utilizing two-color transient absorption microscopy to image melanins in tissue and differentiating eumelanin and pheomelanin. With 810 nm as the pump beam and 740 nm as the probe beam, we demonstrate high SNR imaging of melanin granules within the epidermis and dermis of an invasive melanoma skin sample. Submicrometer features can be well resolved and many important morphological features can be characterized based on the image. We implement epimode imaging and demonstrate its validity using hair samples. With the hair model system, we study in detail the long-lived signal in transient absorption imaging. It is discovered that photothermal effects contribute to the signal significantly when the sample is thin, but long-lived excited state effects are dominant with thick samples.

Two important differences are found between eumelanin and pheomelanin: eumelanin (in black hair) has about a two times larger long-lived excited state lifetime compared to pheomelanin, and the ratio of long-lived signal to short-lived signal is about five times as large for pheomelanin as it is for eumelanin. With these differences, we can expect to use two-color transient absorption as a nonlinear signature in imaging not only melanin distribution changes, but also melanin production changes in human skin tissue with 3-D subcellular resolution in the future, which can be an invaluable diagnostic tool in noninvasive skin imaging for differentiating normal tissue, benign nevi, and melanomas.

References

1. G. N. Stamatas, B. Z. Zmudzka, N. Kollias, and J. Z. Beer, "Noninvasive measurements of skin pigmentation *in situ*," *Pigment Cell Res.* **17**, 618–626 (2004).
2. Z. Huang, H. Lui, X. K. Chen, A. Alajlan, D. I. McLean, and H. Zeng, "Raman spectroscopy of *in vivo* cutaneous melanin," *J. Biomed. Opt.* **9**(6), 1198–1205 (2004).
3. Z. Huang, H. Zeng, I. Hamzavi, A. Alajlan, E. Tan, D. I. McLean, and H. Lui, "Cutaneous melanin exhibiting fluorescence emission under near-infrared light excitation," *J. Biomed. Opt.* **11**, 034010 (2006).
4. M. Rajadhyaksha, M. Grossman, D. Esterowitz, and R. H. Webb, "*In vivo* confocal scanning laser microscopy of human skin—melanin provides strong contrast," *J. Invest. Dermatol.* **104**, 946–952 (1995).
5. M. Rajadhyaksha, S. Gonzalez, J. M. Zavislan, R. R. Anderson, and R. H. Webb, "*In vivo* confocal scanning laser microscopy of human skin II: advances in instrumentation and comparison with histology," *J. Invest. Dermatol.* **113**, 293–303 (1999).
6. G. Pellacani, A. M. Cesinaro, C. Longo, C. Grana, and S. Seidenari, "Microscopic *in vivo* description of cellular architecture of dermoscopic pigment network in Nevi and melanomas," *Arch. Dermatol.* **141**, 147–154 (2005).
7. A. Gerger, S. Koller, T. Kern, C. Massone, K. Steiger, E. Richtig, H. Kerl, and J. Smolle, "Diagnostic applicability of *in vivo* confocal laser scanning microscopy in melanocytic skin tumors," *J. Invest. Dermatol.* **124**, 493–498 (2005).
8. D. S. Gareau, G. Merlino, C. Corless, M. Kulesz-Martin, and S. L. Jacques, "Noninvasive imaging of melanoma with reflectance mode confocal scanning laser microscopy in a murine model," *J. Invest. Dermatol.* **127**, 2184–2190 (2007).
9. K. J. Busam, A. A. Marghoob, and A. Halpern, "Melanoma diagnosis by confocal microscopy: promise and pitfalls," *J. Invest. Dermatol.* **125**, 7–9 (2005).
10. Y. Liu, L. Hong, K. Wakamatsu, S. Ito, B. Adhyaru, C. Y. Cheng, C. R. Bowers, and J. D. Simon, "Comparison of structural and chemical properties of black and red human hair melanosomes," *Photochem. Photobiol.* **81**, 135–144 (2005).
11. S. Ito and K. Wakamatsu, "Quantitative analysis of eumelanin and pheomelanin in humans, mice, and other animals: a comparative review," *Pigment Cell Res.* **16**, 523–531 (2003).
12. S. Takeuchi, W. G. Zhang, K. Wakamatsu, S. Ito, V. J. Hearing, K. H. Kraemer, and D. E. Brash, "Melanin acts as a cause an atypical potent UVB photosensitizer to mode of cell death in murine skin," *Proc. Natl. Acad. Sci. U.S.A.* **101**, 15076–15081 (2004).
13. M. R. Chedekel, S. K. Smith, P. W. Post, A. Pokora, and D. L. Vessell, "Photodestruction of pheomelanin—role of oxygen," *Proc. Natl. Acad. Sci. U.S.A.* **75**, 5395–5399 (1978).
14. T. Ye, L. Hong, J. Garguilo, A. Pawlak, G. S. Edwards, R. J. Nemanich, T. Sarna, and J. D. Simon, "Photoionization thresholds of melanins obtained from free electron laser-photoelectron emission microscopy, femtosecond transient absorption spectroscopy and electron paramagnetic resonance measurements of oxygen photoconsumption," *Photochem. Photobiol.* **82**, 733–737 (2006).
15. M. R. Vincensi, M. d'Ischia, A. Napolitano, E. M. Procaccini, G. Riccio, G. Monfrecola, P. Santoianni, and G. Prota, "Phaeomelanin versus eumelanin as a chemical indicator of ultraviolet sensitivity in fair-skinned subjects at high risk for melanoma: a pilot study," *Melanoma Res.* **8**, 53–58 (1998).
16. T. G. Salopek, K. Yamada, S. Ito, and K. Jimbow, "Dysplastic melanocytic nevi contain high-levels of pheomelanin—quantitative comparison of pheomelanin eumelanin levels between normal skin, common nevi, and dysplastic nevi," *Pigment Cell Res.* **4**, 172–179 (1991).
17. K. Jimbow, S. K. Lee, M. G. King, H. Hara, H. Chen, J. Dakour, and H. Marusyk, "Melanin pigments and melanosomal proteins as differentiation markers unique to normal and neoplastic melanocytes," *J. Invest. Dermatol.* **100**, S259–S268 (1993).
18. L. Chin, "The genetics of malignant melanoma: lessons from mouse and man," *Nat. Rev. Cancer* **3**, 559–570 (2003).
19. D. Fu, T. Ye, T. E. Matthews, G. Yurtsever, and W. S. Warren, "Two-color, two-photon, and excited-state absorption microscopy," *J. Biomed. Opt.* **12**, 054004 (2007).
20. Y. Liu, V. R. Kempf, J. B. Nofsinger, E. E. Weinert, M. Rudnicki, K. Wakamatsu, S. Ito, and J. D. Simon, "Comparison of the structural and physical properties of human hair eumelanin following enzymatic or acid/base extraction," *Pigment Cell Res.* **16**, 355–365 (2003).
21. D. Fu, T. Ye, T. E. Matthews, G. Yurtsever, L. Hong, J. D. Simon, and W. S. Warren, "Two-color excited-state absorption imaging of melanins," *Proc. SPIE* **6424**, 642402 (2007).
22. B. R. Masters, P. T. C. So, C. Buehler, N. Barry, J. D. Sutin, W. W. Mantulin, and E. Gratton, "Mitigating thermal mechanical damage potential during two-photon dermal imaging," *J. Biomed. Opt.* **9**, 1265–1270 (2004).
23. S. M. Mian, S. B. McGee, and N. Melikechi, "Experimental and theoretical investigation of thermal lensing effects in mode-locked femtosecond Z-scan experiments," *Opt. Commun.* **207**, 339–345 (2002).
24. B. Brazzini, G. Hautmann, I. Ghersetich, J. Hercogova, and T. Lotti, "Laser tissue interaction in epidermal pigmented lesions," *J. Eur. Acad. Dermatol. Venereol* **15**, 388–391 (2001).
25. B. Kongshoj, A. Thorleifsson, and H. C. Wulf, "Pheomelanin and eumelanin in human skin determined by high-performance liquid chromatography and its relation to *in vivo* reflectance measurements," *Photodermatol. Photoimmunol. Photomed.* **22**, 141–147 (2006).
26. N. Nagai, Y. J. Lee, N. Nagaoka, M. Gunduz, K. Nakano, T. Nojima, H. Tsujigiwa, E. Gunduz, C. H. Siar, and H. Nagatsuka, "Elemental sulphur and alkali elutable melanin detected in oral melanosis and malignant melanoma by energy-filtering transmission electron microscopy," *J. Oral Pathol. Med.* **31**, 481–487 (2002).
27. N. Kollias, "The spectroscopy of human melanin pigmentation," *J. Invest. Dermatol.* **102**, 268–268 (1994).
28. H. Ozeki, S. Ito, K. Wakamatsu, and A. J. Thody, "Spectrophotometric characterization of eumelanin and pheomelanin in hair," *Pigment Cell Res.* **9**, 265–270 (1996).
29. T. Ye, G. Yurtsever, M. Fischer, J. D. Simon, and W. S. Warren, "Imaging melanin by two-photon absorption microscopy," *Proc. SPIE* **6089**, 60891X (2006).
30. K. Teuchner, J. Ehlert, W. Freyer, D. Leupold, P. Altmeyer, M. Stucker, and K. Hoffmann, "Fluorescence studies of melanin by step-wise two-photon femtosecond laser excitation," *J. Fluoresc.* **10**, 275–281 (2000).
31. C. Y. Dong, C. Buehler, T. C. So, T. French, and E. Gratton, "Implementation of intensity-modulated laser diodes in time-resolved, pump-probe fluorescence microscopy," *Appl. Opt.* **40**, 1109–1115 (2001).